Journal of Photochemistry & Photobiology, A: Chemistry 466 (2025) 116393

Contents lists available at ScienceDirect

Journal of Photochemistry & Photobiology, A: Chemistry

journal homepage: www.elsevier.com/locate/jphotochem

# Theoretical regulation of firefly bioluminescence spectra: Exploring new frontiers in NIR-II imaging

Jinyu Wang [a], Deping Hu [b], Ya-Jun Liu [a,b,*]

[a] Key Laboratory of Theoretical and Computational Photochemistry, Ministry of Education, College of Chemistry, Beijing Normal University, Beijing 100875, China
[b] Department of Chemistry, Faculty of Arts and Sciences, Center for Advanced Materials Research, Beijing Normal University, Zhuhai 519087, China

ARTICLE INFO

*Keywords:*
Bioluminescence imaging
NIR-II
Mutation
QM/MM

ABSTRACT

Firefly bioluminescence (BL) imaging holds significant promise for non-invasive, real-time monitoring of biological processes. To improve its efficiency, considerable efforts have been made to achieve red-shifting of the emission wavelength. In this work, we systematically investigated the fluorescence properties of the light emitter oxyluciferin (**oLu**) dependent on the electrostatic effects using the TD DFT method. **oLu** is a typical donor–acceptor (D-A) charge transfer system, with the benzothiazole group acting as the electron donor and the thiazole group as the electron acceptor. Therefore, we focused on the significant impact of external charges on the fluorescence wavelength ($\lambda_F$), where the negative charge around the benzothiazole (donor) and/or the positive charge around the thiazole (acceptor) side promotes a red-shift in $\lambda_F$. Basing on these insights, we theoretically explored modifications to the **oLu** structure and mutations in luciferase to enhance D and A properties of **oLu** for facilitating the $\lambda_F$ red-shift. Besides, we also inserted conjugation structures between D and A of **oLu** to format D-π-A systems for further red-shifting the $\lambda_F$. By integrating **oLu** modifications with luciferase mutations, we successfully designed a new **nova-I351D** using MD and QM/MM methods, a bioluminescent system that emits brightly in the near-infrared II (NIR-II) region. This system demonstrates significant potential for deep tissue imaging, providing a promising advancement in bioluminescence-based imaging technologies.

## 1. Introduction

Compared with the fluorescence imaging [1], bioluminescence (BL) imaging eliminates the need for external light sources by generating light signals through enzymatic reactions between luciferase and luciferin.[2] This technique allows for non-invasive, real-time monitoring of tumor growth, metastasis, and cellular behavior, offering a high signal-to-noise ratio for therapeutic studies [3–6]. Among the various BL systems [7–12], firefly BL stands out for its high quantum yield, making it particularly valuable in applications such as bioassays and bioimaging [9]. The luminescence mechanism of firefly BL is illustrated in Scheme 1. Under the catalysis of luciferase, D-luciferin undergoes an adenylation reaction with ATP and $Mg^{2+}$, forming an intermediate D-adenylluciferin. D-adenylluciferin intermediate subsequently reacts with oxygen to produce the first excited-state ($S_1$) oxyluciferin, which emits yellow-green light as it deexcitates to its ground state ($S_0$) [2,13–15]. However, the emission wavelength of firefly BL is 557 nm [16], which falls within the absorption and scattering range of tissues, limiting its effectiveness for deep tissue imaging.

To overcome this limitation and enhance the utility of firefly BL for in vivo applications, researchers have focused on developing bioluminescent systems with lengthening BL emission wavelengths through structural modifications of luciferin [17–42] or mutations of luciferase [16,33,43–48]. Various synthetic luciferin analogues and luciferase mutants have been developed and reviewed [12,49–51]. Meanwhile, a series of BL probes based on the firefly luciferin scaffold have been developed, utilizing the caged luciferin strategy for enzyme activity detection, thereby enabling real-time monitoring of biological processes through in vivo imaging [3,52–55].

Despite the significant progress made in this field, there are still the following limitations in current research: (1) For luciferin modifications, some experimental modifications have been found to negatively affect BL imaging. For instance, replacing the benzothiazole ring with a naphthalene ring caused a blue shift in BL to 524 nm [24], while substituting the carboxyl group on the thiazole ring with a hydrogen atom rendered the molecule non-luminescent [27]. This illustrates the

* Corresponding author at: Key Laboratory of Theoretical and Computational Photochemistry, Ministry of Education, College of Chemistry, Beijing Normal University, Beijing 100875, China.
*E-mail address:* yajun.liu@bnu.edu.cn (Y.-J. Liu).

https://doi.org/10.1016/j.jphotochem.2025.116393
Received 19 January 2025; Received in revised form 4 March 2025; Accepted 16 March 2025
Available online 19 March 2025

randomness of the experimentally synthesized direction. Theoretically, the key to modulating BL emission wavelength lies in adjusting the light emitter, namely the fluorescence wavelength ($\lambda_F$) of oxyluciferin [56]. Various oxyluciferin analogues have been designed and studied [57–61], with a focus on the color tuning mechanisms involving substituents [57,59,60] or the conjugation length of the system [60]. However, most of these studies have not considered the actual luciferase environment [57–59,61], or the oxyluciferin analogues involved have not been systematically explored [57–60]. (2) For mutations of luciferase, experimentally, large-scale site-directed mutagenesis [16] and high-throughput screening [45] remain exploratory, lacking effective strategies for the discovery of the desired mutants. Theoretically, the relationship between the structure and luminescent wavelength of certain mutants has been discussed [60,62,63]. However, the limited scope of the studied variants has prevented the formulation of generalizable conclusions.

The objective of this study is to systematically develop a highly efficient bioluminescent probe that emits in the near-infrared II (NIR-II) region. Like previous theoretical studies [58–60], our focus is on lengthening the $\lambda_F$ of the light emitter, oxyluciferin. Oxyluciferin exists in various forms [64,65], among which the anionic keto form has been verified to be the main light emitter [66,67]. Therefore, for clarity and simplicity, the anionic keto form of oxyluciferin, henceforth designated as **oLu** (Scheme 2), will serve as the mother substrate of our investigation. The general approach to lengthening the $\lambda_F$ of **oLu** involves modifying **oLu** and mutating the luciferase. One, the modification of **oLu**. Theoretical analysis identifies **oLu** as a typical donor–acceptor (D-A) system, with the benzothiazole moiety acting as the electron donor and the thiazole ring serving as the electron acceptor. To achieve red-shifted emission, we enhanced the electron donating/accepting effects by introducing the related substituents. Additionally, extending π-conjugation to form a D-π-A system was pursued to further promote red-shifting. Two, the mutation of wild-type luciferase. The wild-type luciferase was mutated, and the fluorescence properties of the selected **oLu** substrates in the wild and mutant luciferases were investigated. Notably, prior to the modification of **oLu** and the mutation of wild-type luciferase, we first investigated the influence of external point charges on the fluorescence spectral properties of **oLu**. The analysis of electrostatic effects provided crucial guidance for selecting substituents and luciferase mutations in our study. Fortunately, through these strategies, we successfully designed a desired bioluminescent system, named **nova-I351D**, which emits bright light in the NIR-II region. **nova** is the structure of the substrate after substitution and conjugation modifications of **oLu**, **I351D** is the luciferase variant where Ile351 is changed to Asp. The design concept of **nova-I351D** is described in Scheme 2.

## 2. Computational methods

*Quantum Mechanics (QM) Calculations.* The time-dependent density functional theory (TD-DFT) theory was employed in all QM calculations [68]. The long-range-corrected functional CAM-B3LYP [69] was employed for a better description of the charge-transfer transitions of **oLu** and its analogues in their excited states, and the dispersion effects were considered [70]. The geometries of **oLu** and its analogues in the $S_1$ state were optimized at the TD-DFT/CAM-B3LYP/6–31 + G** level. Based on the optimized geometries, the calculated $\lambda_F$ of **oLu** using 6–31 + G**, 6–311++G** and ma-def2-TZVP basis sets were 536, 537 and 539 nm, respectively. The calculated $\lambda_F$ using ma-def2-TZVP basis set is closer to the experimental value of 557 nm [16]. Therefore, the spectroscopic properties including $\lambda_F$, oscillator strength ($f$), vertical emission energy ($E_v$), transition dipole moment ($\boldsymbol{\mu_T}$) and permanent dipole moment ($\boldsymbol{\mu}$) of the $S_0$ and $S_1$ states were determined at the TD-DFT/CAM-B3LYP/ma-def2-TZVP level. To investigate the electrostatic effect on the spectra, external point charges with positive or negative charges were introduced and placed along the bonding direction of the skeleton atoms of optimized **oLu**, at a distance of 1.5 Å from the skeleton atoms for single-point calculations, as shown in the top diagram of Scheme 2. Considering that the active site of firefly luciferase is a non-polar environment, all QM calculations were performed using a dielectric constant of 4 to simulate the enzyme's environment [71,72], with the implicit solvent model being PCM (Polarizable Continuum Model) [73]. All QM calculations were performed with the Gaussian 09 software [74]. The electronic transition analysis was performed using the Multiwfn software [75].

*Setup of Computational Systems.* The crystallographic structure of the wild-type *photinus pyralis* firefly luciferase (WT, PDB ID: 4G36) was utilized for model construction [76]. The structure comprises two same chains, A and B, both bound to the adenylate analogue 5′-O-[N-dehydroluciferyl)-sulfamoyl]-adenosine (DLSA), as shown in Fig. S1 of supporting information. For the sake of computational efficiency, only chain B was retained in the model. Missing residues were added by the ModLoop online server [77,78]. Based on the processed crystal structure, protein models for two luciferase mutants, I351A and I351D, were subsequently constructed. The DLSA in these crystal structures (WT, I351A and I351D) were modeled as **oLu** and adenosine bonophosphate (AMP) or **nova** and AMP, resulting in a total of six distinct systems: **oLu-WT**, **oLu-I351A**, **oLu-I351D**, **nova-WT**, **nova-I351A** and **nova-I351D**. The protonation states of titratable residues (histidine, glutamic acid and aspartic acid) were determined with the online H++ program [79]. The Amber Parm99SB force field [80] was employed for protein residues, while the general amber force field (GAFF) [81] was used to describe **oLu** and **nova**. Charge parameters of **oLu** and **nova** were obtained by using the RESP method [82] at the HF/6-31G* level with the Gaussian 09 software. The parmchk2 utility from AmberTools was used to generate missing force field parameters. The force field parameters for AMP were adopted from the work by Navizet et al. [83] Sodium ions were added to the protein surface to neutralize the overall charge of the systems. The resulting system was solvated in a rectangular box of TIP3P [84] waters extending up to a minimum cutoff of 12 Å from the protein surface.

*Molecular Dynamics (MD) Simulation of the Systems.* After proper setups, every system was then equilibrated in the following way: (1) the energy was minimized by using a combination of the steepest descent and conjugate-gradient methods; (2) the system was heated from 0 K to 300 K over a 400 ps period in the NVT ensemble, with a weak constraint applied to the protein backbone atoms; (3) the density was equilibrated for 1 ns at a target temperature of 300 K and a pressure of 1.0 atm, utilizing an isothermal-isobaric Langevin thermostat [85] and Berendsen barostat [86] with a collision frequency of 2 $ps^{-1}$ and a pressure relaxation time of 1 ps; (4) an additional 3 ns equilibration was

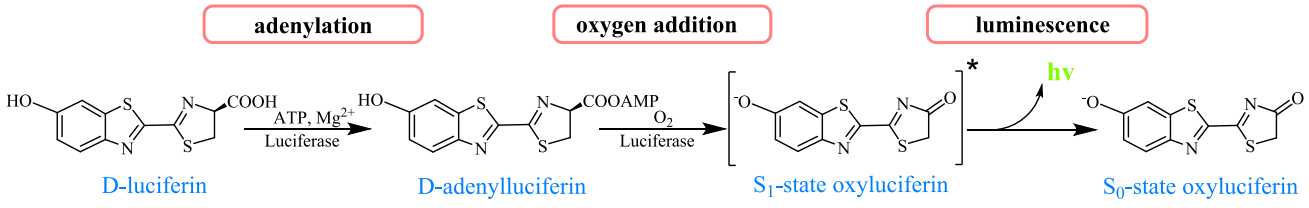


**Scheme 1.** A brief illustration of firefly bioluminescence process.

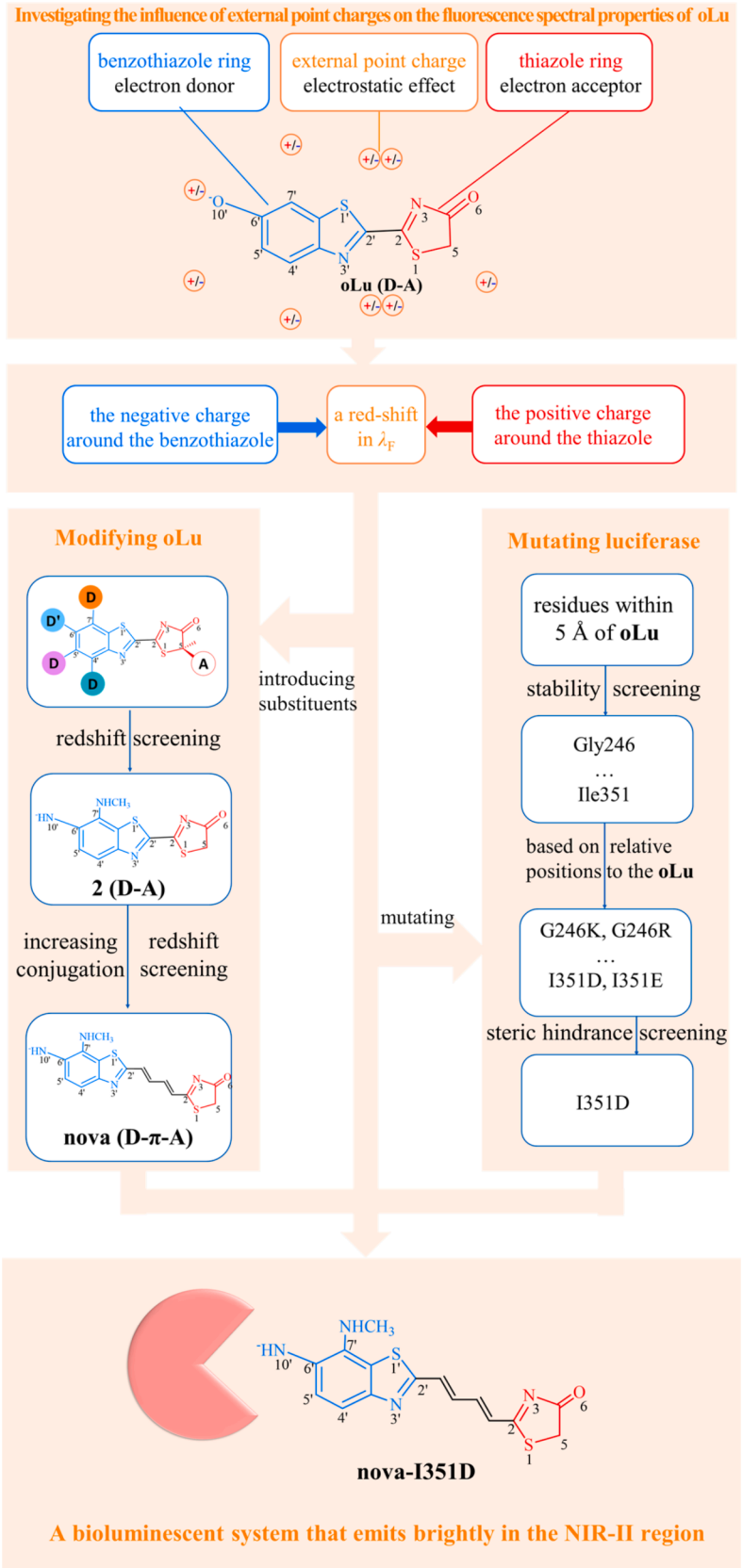


**Scheme 2.** Design concept from oLu to nova-I351D.

performed under the NPT ensemble to get a well-settled pressure and temperature. (5) a 100 ns MD simulation was performed. Nonbonded interactions were treated with the Particle Mesh Ewald method with a cutoff of 12 Å [87]. The covalent bonds containing hydrogen atoms were constrained with the SHAKE algorithm, enabling a 2-fs integration step. All MD simulations were performed with the AMBER21 software [88]. Based on the MD trajectory of **oLu-WT,** the contribution of the residues surrounding the **oLu** to the binding energy was calculated using the molecular mechanics/Poisson Boltzmann surface area (MM/PBSA) method with the mmpbsa.py script in AMBER21, which was subsequently used to identify suitable residues for selective mutations in luciferase.

*Quantum Mechanics and Molecular Mechanics (QM/MM) Calculations.* The equilibrated geometry from the MD trajectory was used as the initial input structure for the QM/MM calculations. For six systems, **oLu** or **navo** was put into the QM region, while other atoms were put into the MM region. For the geometry optimizations in the $S_1$ states of six systems, the TD CAM-B3LYP/6–31 + G** method was used for the QM region. The atoms within 5 Å of **oLu** or **nova** in the MM region were allowed to relax during the geometry optimization process. For the discussion about fluorescence properties, the TD CAM-B3LYP/ma-def2-TZVP method was used for the QM region. All QM/MM calculations were carried out using the ChemShell software [89–91], which integrates ORCA [92] for the QM region and DL_POLY [93] for the molecular mechanical (MM) region. The TD-DFT method was employed for the QM region of QM/MM calculations, while the Amber Parm99SB force field [80] was used to describe the MM protein environment. To include the polarization effect of the MM region on the QM region, the electronic embedding scheme was employed in the QM/MM calculations [94].

## 3. Results and discussion

### 3.1. Fluorescence spectral properties of oLu and the electrostatic effects on fluorescence spectrum based on the optimized $S_1$-state geometry of oLu

The calculated fluorescence spectrum of **oLu**, shown in Fig. 1**A**, exhibits a yellow-green emission peak at 539 nm corresponding to the $S_1 \rightarrow S_0$ transition. This calculated value is in close agreement with the experimental fluorescence emission peak, which is observed around 557 nm [16]. The emission primarily arises from the de-excitation process, where the electron relaxes from the lowest unoccupied molecular orbital (LUMO, π*) to the highest occupied molecular orbital (HOMO, π). The HOMO is predominantly localized on the benzothiazole ring, while the LUMO is delocalized over the entire molecule (Fig. 1**B**). This is consistent with the charge distribution observed in the $S_0$ and $S_1$ states of **oLu**: the benzothiazole and thiazole rings exhibit charge distributions of −0.717 and −0.283 in the $S_0$ state, and −0.516 and −0.484 in the $S_1$ state, respectively (**Table S1**). Thus, during the transition from $S_0$ to $S_1$, the electron density on the benzothiazole ring decreases, while that on the thiazole ring increases, indicating a net electron transfer from the benzothiazole ring to the thiazole ring. Further hole-electron analysis (Fig. 1**C**) supports this conclusion [95]. Additionally, dipole moment analysis **(**Fig. 1**D)** reveals that the dipole moments in both the $S_0$ and $S_1$ states have components directed towards the thiazole ring, with the component in the $S_1$ state being smaller than that in the $S_0$ state. Since the dipole moment typically points from the negative charge center to the positive charge center, this is consistent with the charge distribution, where the benzothiazole ring carries a greater negative charge than the thiazole ring in both states. Notably, the negative charge on the benzothiazole ring is smaller in the $S_1$ state compared to that in the $S_0$ state. The difference in dipole moment magnitude is 5.68 Debye (D), directed from the thiazole ring to the benzothiazole ring, providing further evidence of electron transfer from the benzothiazole ring to the thiazole ring, in agreement with the previous analysis in the text, as shown in Fig. 1**B and 1C** and **Table S1**.

The analysis above reveals that **oLu** is a prototypical donor–acceptor (D-A) charge transfer system, with the benzothiazole ring serving as the electron donor and the thiazole ring as the electron acceptor. To investigate the electrostatic effects on its spectral properties, point charges were introduced 1.5 Å away from the bonding direction of atoms in the backbone of **oLu**, as shown in Scheme 2. The results demonstrate that placing negative point charges near the C4′, C5′, C6′, C7′, and S1′ positions, or positive charges near the C5, S1, N3, and N3′ positions, induces a redshift in $\lambda_F$, with the magnitude of the shift increasing with the amount of charge (Fig. 2**A and 2B**). Conversely, $\lambda_F$ exhibits a blueshift when the charges are reversed. These findings suggest that a redshift occurs when negative point charges are positioned around the donor side (benzothiazole ring) or positive charges around the acceptor side (thiazole ring), while the opposite charge placements

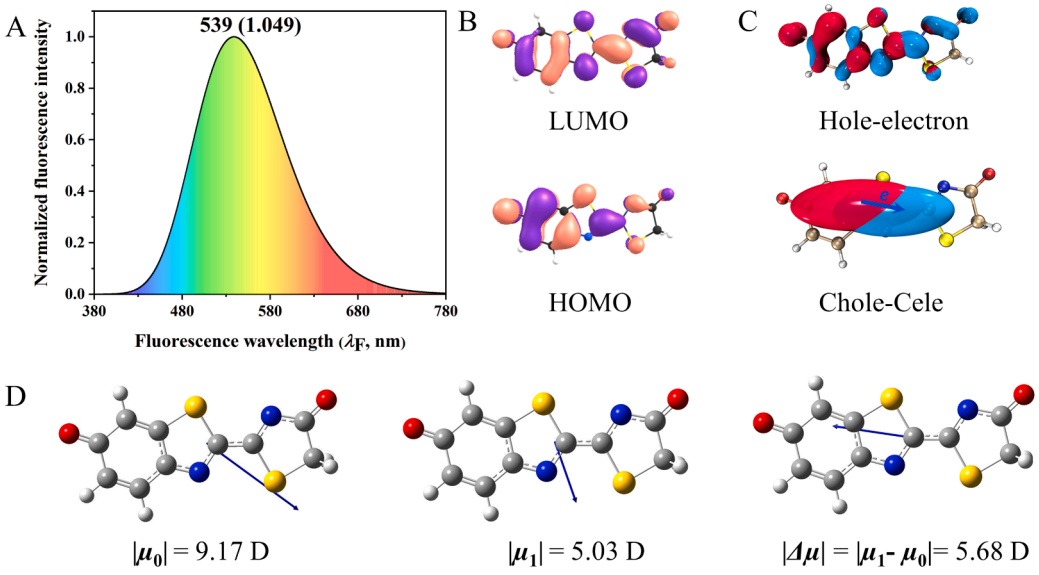


**Fig. 1.** (A) The calculated fluorescence spectrum of oLu. (B) The major frontier molecular orbitals of oLu. (C) The hole-electron distribution map and its smoothed counterpart of $S_0 \rightarrow S_1$ transition of oLu, with the red and blue parts representing holes and electrons, respectively. (D) The permanent dipole moments of the ground ($\mu_0$) and first excited ($\mu_1$) states and the difference between them ($\Delta\mu$) of oLu.

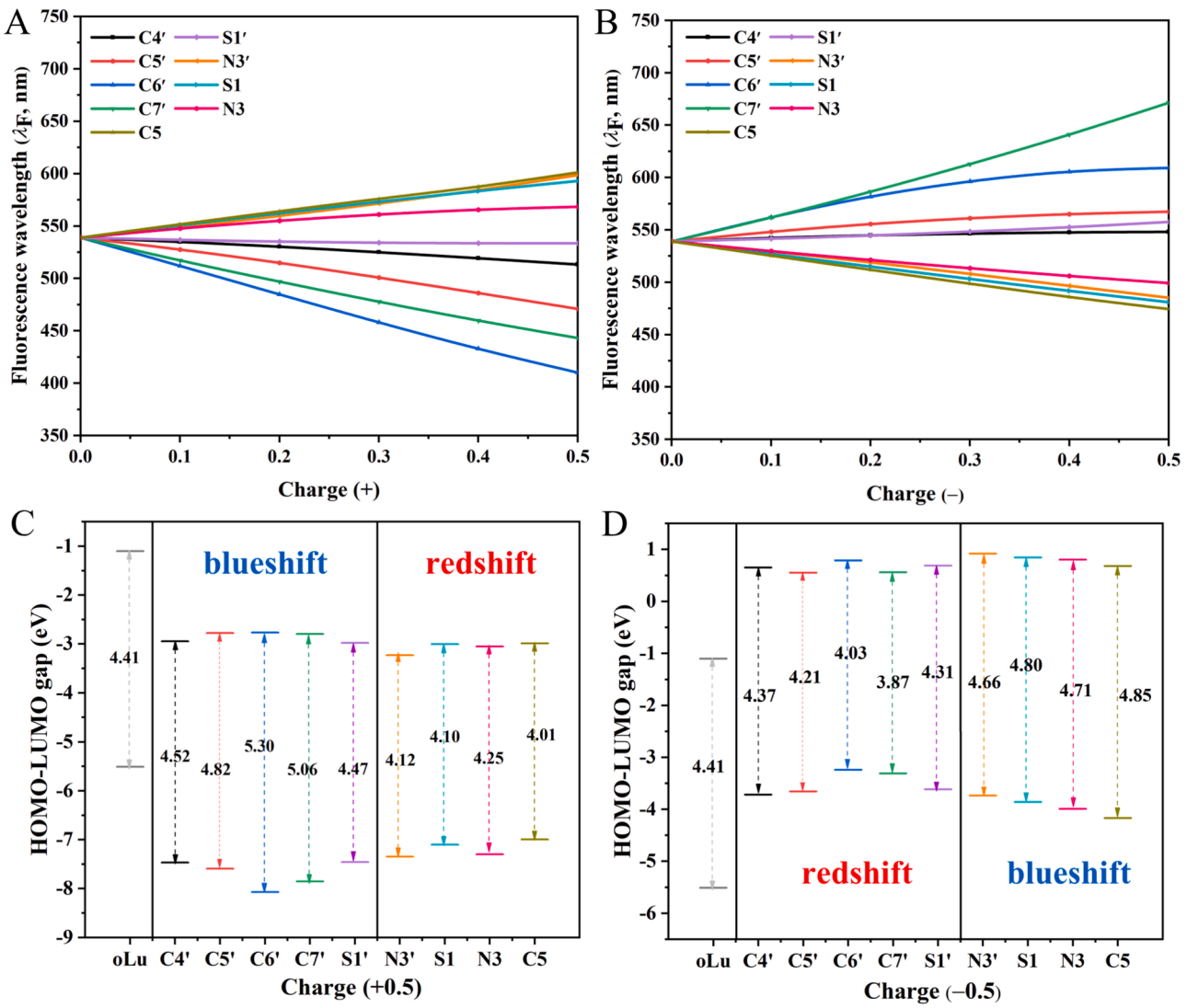


**Fig. 2.** Effect of external (A, C) positive and (B, D) negative point charges on fluorescence wavelength ($\lambda_F$, nm) and HOMO-LUMO gap of oLu.

lead to a blueshift.

The behavior above can be attributed to the electrostatic interactions caused by the point charges, which alter the intramolecular electron distribution, thereby changing the energy levels of the molecular orbitals and affecting the HOMO-LUMO gap (Fig. 2**C and D**). The molecule, being overall negatively charged, experiences repulsive interactions between the external negative charges and the internal electrons, which elevates both the HOMO and LUMO orbital energies. In contrast, positive charges attract the electrons, lowering these orbital energies. Consequently, placing a negative charge around the donor side (benzothiazole ring) raises the HOMO energy significantly, as the electron density is primarily localized on the donor side, while the LUMO energy increases to a lesser extent due to its delocalization across the entire molecule. This results in a reduced HOMO-LUMO gap and a redshift in the $\lambda_F$. Similarly, placing a positive charge around the acceptor side (thiazole ring) lowers the LUMO energy more significantly than the HOMO energy, leading to a decrease in the HOMO-LUMO gap and a redshift in $\lambda_F$. In addition to the aforementioned phenomena, we found that, the largest redshift in $\lambda_F$ occurs when a negative charge is placed near the C7′ position. This can be attributed to the significant difference in electronic density around the C7′ region between the HOMO and LUMO orbitals. The negative charge leads to a substantial increase in the energy of the HOMO, while the LUMO energy increases only marginally, resulting in a greatly reduced HOMO-LUMO gap.

The influence of external charges on luminescence intensity is shown in Fig. S2. Compared to the effect of external charges on luminescence wavelength, the increase or decrease in luminescence intensity does not have a clear relationship with the position of the point charge relative to **oLu**. This is due to the combined contribution of changes in $E_v$ and $\boldsymbol{\mu}_T$ caused by the change in the charge distribution (**Figs. S3 and S4**).

### 3.2. *Design of the bioluminescent system in NIR-II reigon*

#### 3.2.1. *Modifying oxyluciferin*

*Introducing substituents.* Building on the findings discussed above, electrostatic effects have proven to be an effective approach for tuning $\lambda_F$. Consequently, electron-donating and electron-withdrawing substituents were introduced at specific positions to generate **oLu** analogues exhibiting redshifted fluorescence characteristics. Considering that substitution with heteroatoms may disrupt the original backbone of fluorescein, potentially leading to a decrease or complete quenching of fluorescence [39], electron-donating substituents were introduced at the C4′, C5′, C6′, and C7′ positions on the benzene ring, while electron-withdrawing substituents were introduced at the C5 position on the thiazole ring. Based on the Hammett $\sigma_p$ constants [96], strong electron-donating substituents include –$NHCH_3$, –$NH_2$, –OH, and –$OCH_3$, while strong electron-withdrawing substituents include –$NO_2$, –CN, –$CF_3$, and –Br. The **oLu** analogues formed by these substitutions are shown in

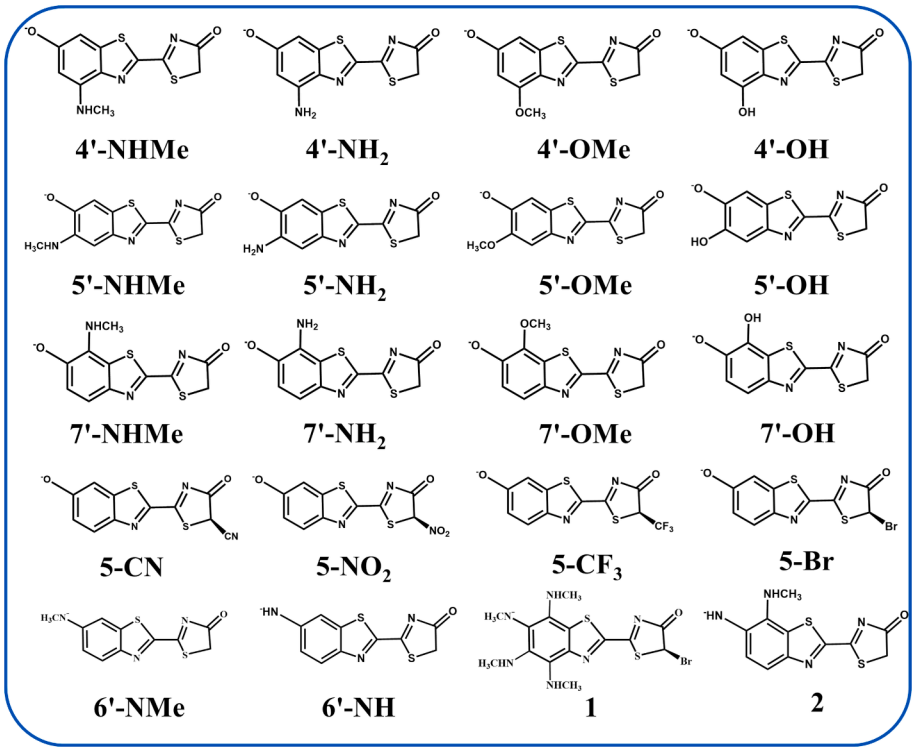


**Fig. 3.** Molecular structures and abbreviations of oLu analogues.

Fig. 3. For some analogues, two or more conformations can be formed through altering the orientation of the substituents, we only selected the most stable conformation with the lowest energy for subsequent discussion. The details of the molecular structures and relative energies of all conformations are shown in **Figs. S5–S8**.

The $\lambda_F$ and $f$ of **oLu** and its analogues, based on their optimized $S_1$-state geometries, are presented in Fig. 4. The calculated and experimental $\lambda_F$ for **oLu**, 6′-NMe, and 6′-NH are 539 and 557 nm, 597 and 615 nm [97], and 585 and 596 nm [40], respectively. The close agreement between the calculated values and the experimental data validates the reliability of the computational method. Notably, with the exception of the 5′-OH derivative, all **oLu** analogues exhibited a redshift in $\lambda_F$, with the most significant redshift occurring at the C7′ substitution. This is consistent with our previous findings, which showed that placing a negative point charge at the C7′ position results in the largest redshift. Furthermore, among the substitutions at the C4′, C5′, C6′, and C7′ positions, the analogues with –$NHCH_3$ substitution exhibited the most pronounced redshift. These results confirm the effectiveness of the design strategy, where electron-donating and electron-withdrawing substituents replace negative and positive point charges, respectively, and the substituents are selected based on Hammett constants to modulate the $\lambda_F$.

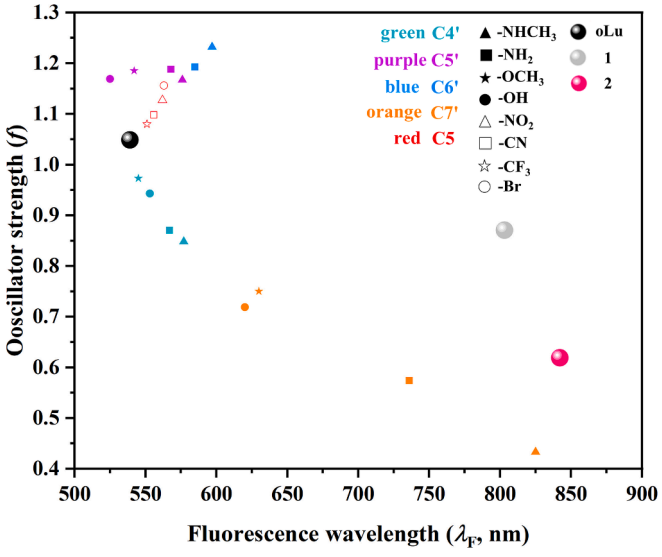


**Fig. 4.** The fluorescence wavelength ($\lambda_F$, nm) and oscillator strength ($f$) of oLu and its analogues.

Building on these observations, **oLu** analog **1** was designed to achieve a maximum redshift. However, its $\lambda_F$ of 803 nm was shorter than that of the single-substituted **7′-NHMe** derivative, suggesting that a higher degree of substitution does not always lead to a greater redshift. This non-linear relationship may be attributed to the combined effects of spatial and electronic effects. As shown in Fig. S9, frontier molecular orbital analysis and hole-electron analysis indicate that the donor-side electron-donating substituents and the acceptor-side electron-withdrawing substituents induce charge transfer within the molecule, promoting electron delocalization. However, the geometric analysis shows that multiple substitutions on the donor side disrupt the planar conjugation structure of the molecule, which hinders the delocalization of electrons of **oLu** anlog **1**. Therefore, given that substitutions at the C4′, C5′, and C5 positions can only make a relatively minor redshift effect, so we next only focus on the substituting at the C6′ and C7′ positions. Furthermore, considering steric effects and experimental evidence that amino substitution at C6′ enhances enzyme affinity,[11] **oLu** analog **2** was designed, exhibiting the best performance among oLu analogues designed through substituent introduction in Fig. 3. It achieves a maximum redshift with $\lambda_F$ of 842 nm and an emission intensity of 58.9 % relative to **oLu**. The observed redshift can be attributed to the introduction of –$NHCH_3$ (at the C7′ position) and –NH (at the C6′ position) substituents, which form p-π conjugation with the benzene ring. This conjugation effect enhances the electron distribution within the molecule, leading to a redistribution of electron density, thereby influencing the molecular spectral properties. Simultaneously, these electron-

donating substituents further increase the electron-donating ability of the benzothiazole ring through electron-donating induction. These effects lower the HOMO-LUMO gap, ultimately leading to the observed redshift in fluorescence emission.

*Enhancing conjugation.* Fluorescent dyes typically exhibit a redshift in their emission spectra as a result of the extension of their π-conjugated systems. Similarly, we aimed to induce a redshift in **oLu** by incorporating conjugated linkages between the benzothiazole and thiazole rings, thereby creating a D-π-A system. Considering that the conjugation length not only affects the spectral properties but also influences the affinity with enzymes [98], we investigated three **oLu** analogues—**3**, **4**, and **5**, as shown in Table 1. These analogues were modified by inserting a single double bond, a phenyl ring, and two double bonds between the benzothiazole and thiazole rings, respectively. The optimized geometries and relative energies of analog **3** with different conformers in $S_1$ are depicted in Fig. S10. Among the four conformers, which include two cis (***cis*-u** and ***cis*-d**) and two trans (***trans*-u** and ***trans*-d**) forms, the trans conformers are more stable. In particular, the ***trans*-u** conformer has the lowest relative energy and is considered the most stable configuration. Its $\lambda_F$ is 647 nm, which closely matches the experimental value of 670 nm [34], and thus ***trans*-u** is identified as the most probable conformer for analog **3**. Similarly, for analog **5**, the most stable trans conformer among the eight configurations is regarded as the most likely conformation (Fig. S11). All subsequent discussions are based on the most stable conformers. The $\lambda_F$ values of analogues **3**, **4**, and **5** show a redshift compared with the one of **oLu** (Table 1), due to increased electron delocalization resulting from the extension of the conjugated system, which in turn reduces the energy gap between the ground and excited states. Considering both $\lambda_F$ and *f*, analog **5** exhibits the best performance among analogues **3**, **4**, and **5**. It shows a redshift of approximately 200 nm in $\lambda_F$ and an emission intensity enhanced by nearly 80 % relative to **oLu**.

*Designing NIR-II **oLu** analogue, **nova**.* In the above, the fluorescence properties of **oLu** analogues, based on their optimized $S_1$-state geometries, were systematically investigated using QM method by introducing various substituents and extending the conjugation length, both of which led to redshifts in their $\lambda_F$. Among all the modified compounds, **oLu** analogues **2** and **5** exhibited the most significant redshift and were therefore selected for further investigation. Based on the observed structure–property relationship and incorporating the characteristics of **2** and **5**, a novel analogue named **nova** was designed, see Scheme 2. The fluorescence properties of **nova,** based on its optimized $S_1$-state geometry, are summarized in Table 2. Remarkably, **nova** exhibits strong near-infrared emission within the NIR-II region in an environment with a dielectric constant of 4.0, a property that holds significant promise for advanced biological imaging applications. Given that the primary objective is the development of a bioluminescent probe, we extended our investigation to evaluate the fluorescence behavior of **nova** in the context of the luciferase using QM/MM method for considering the influence of protein environment. The detailed fluorescence data is provided in Table 2. Notably, **nova** exhibits a $\lambda_F$ of 1066 nm, which corresponds to the NIR-II region, making it an ideal candidate for in vivo imaging applications. The key molecular interactions in WT that govern the fluorescence properties of **nova** are depicted in Fig. S12. On the benzothiazole ring side, Arg218 is positioned in close proximity to the C4′ and C5′ sites, exerting a weak electrostatic attraction toward **nova**. Arg337 and a water molecule are near the C6′ positions, forming stable hydrogen bonds with **nova**. On the thiazole ring side, Lys529 interacts with **nova** through a hydrogen bond network facilitated by a water molecule, and His245 connects with **nova** by a direct hydrogen bond. These hydrogen bond networks collectively enforce a planar conformation for **nova**, which is essential for its optimal fluorescence emission.

**Table 1**
Calculated fluorescence wavelengths ($\lambda_F$, nm) and oscillator strength (*f*) of oLu analogues 3, 4, and 5, along with their corresponding experimental fluorescence wavelength (*Exp*. nm).

| | $\lambda_F$ | *f* | *Exp.* |
|---|---|---|---|
| 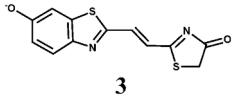 **3** | 647 | 1.401 | 670 [34] |
| 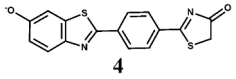 **4** | 631 | 1.509 | |
| 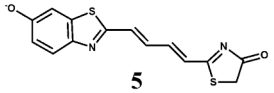 **5** | 724 | 1.878 | |

**Table 2**
At the TD CAM-B3LYP/ma-def2-TZVP and TD CAM-B3LYP/ma-def2-TZVP/MM computational level, calculated fluorescence wavelength ($\lambda_F$, nm) and oscillator strength (*f*) of oLu and nova in environments with a dielectric constant (ε) of 4.0 and in the context of luciferase, along with the corresponding experimental wavelength of oLu (*Exp*. nm).

| | **oLu** | | | **nova** | |
|---|---|---|---|---|---|
| | $\lambda_F$ | *f* | *Exp.* | $\lambda_F$ | *f* |
| ε = 4.0 | 539 | 1.049 | 557 [16] | 1070 | 1.333 |
| WT | 525 | 0.610 | 557 [16] | 1066 | 0.411 |
| I351A | 542 | 0.596 | 573 [16] | 1087 | 0.379 |
| I351D | 543 | 0.557 | – | 1123 | 0.347 |

### 3.2.2. Mutating luciferase

The protein environment significantly influences the BL color, with the microenvironment near luciferin playing a critical role in tuning the emission wavelength [16,99]. To achieve a further redshift in the bioluminescent system, luciferase mutations were strategically applied. Initially, the contribution of the residues surrounding the **oLu** to the binding energy were studied (Fig. S13). The results indicated that charged residues, Arg218 and Lys529, had a substantial impact on the binding energy, which is consistent with experimental observations [16]. Therefore, we did not make mutations to these residues to maintain protein stability. Subsequently, based on the conclusions drawn from the spectral electrostatic effects—where the negative charge on the donor side and the positive charge on the receptor side induce a redshift in fluorescence—we proceeded to mutate the residues based on their relative positions to the **oLu**. It was found that the mutations of Gln338 to Asp or Glu, as well as Ile351 to Asp or Glu, encounter relatively small steric hindrance (Fig. S14). Considering that experimental data are only available for the Ile351 to Ala mutation [16], the fluorescence properties of **oLu** in WT, I351A, and I351D were investigated for comparison, ensuring the reliability of the calculations.

The fluorescence properties of **oLu** in WT, I351A and I351D, based on their optimized $S_1$-state geometries at the TD CAM-B3LYP/6–31 + G**/MM level, are listed in Table 2**.** Compared with the $\lambda_F$ of **oLu** in WT, the $\lambda_F$ of oLu exhibits a red shift in both I351A and I351D, with the shift in I351A matching experimental observations [16]. This red shift is attributed to microenvironmental changes induced by the I351 mutation, which modulate **oLu**'s electronic structure. Specifically, the I351 mutation alters the electrostatic potential distribution within the active site (Fig. S15A) and induces conformational changes in the protein (Fig. S15B). These changes, driven by electrostatic interactions and hydrogen-bonding networks, result in a conformational adjustment of **oLu**. Key interactions at the binding site are shown in Fig. S16, where **oLu** interacts with surrounding water molecules and residues such as Lys529 and His245 through hydrogen bonds, and forms electrostatic attractions with positively charged residues, including Arg218, Arg337, and Lys529. In I351A, the substitution of Ile with Ala reduces steric

hindrance, allowing surrounding residues to move closer. This brings Phe247 closer to the benzothiazole ring, enhancing π–π stacking interactions (Fig. S16B). In I351D, the negatively charged Asp residue causes electrostatic repulsion with **oLu**, which enhances the electron-donating ability of the benzothiazole ring. Additionally, Asp351 forms an electrostatic attraction with Arg337, causing Arg337 to shift upward and move closer to nearby water molecules. These water molecules form hydrogen bonds with Arg337, reducing its electron-withdrawing effect on the benzothiazole ring (Fig. S16C).

### *3.3. Designing NIR-II bioluminescent systems with longer fluorescence wavelengths through introducing nova in luciferase mutants*

The $\lambda_F$ of **oLu** exhibited a redshift in both I351A and I351D. Therefore, the fluorescence properties of **nova** in I351A and I351D were also investigated, as summarized in Table 2. Similar to the case of **oLu**, compared to the $\lambda_F$ of **nova** in WT, those also exhibited a red shift in I351A and I351D, which can be attributed to microenvironmental changes, including alterations in the electrostatic potential (Fig. S17A) and protein conformation (Fig. S17B) induced by the I351 mutation, thereby modulating the electronic structure of **nova**.

For **nova** in I351A, the key interactions at the binding site (Fig. S18) reveal that, in addition to hydrogen bonding with water molecules and Lys529, Arg337 and Arg218 relocate from a lateral position near **nova**'s benzothiazole ring to an axial position above it, weakening their electrostatic attraction to **nova**'s donor side. Meanwhile, Lys529 moves closer to the acceptor side, strengthening its electrostatic attraction to **nova**'s receptor side.

For **nova** in I351D (Fig. 5), the key interactions at the active site indicate that, in addition to hydrogen bonding with water molecules and residues such as Arg218 and Lys529, **nova** also experiences electrostatic attractions with Arg218, Arg337, and Lys529, as well as electrostatic repulsion with Asp351. Asp351, located on the donor side of **nova**, enhances its electron-donating ability. This is likely a key factor contributing to the longer wavelength of **nova** in I351D compared to I351A. Furthermore, the redshift of **nova** in I351D is significantly greater than that of **oLu** in I351D, compared to their respective wild-type counterparts. Analysis of key interactions at the active site reveals that, for **oLu** in I351D, the positively charged residue Lys529 is located near the receptor side and forms a hydrogen bond with **oLu**. In contrast, for **oLu** in I351D, Lys529 moves farther from the receptor side and forms a hydrogen bond network with **oLu** through a water molecule. However, for **nova** in I351D, the situation is reversed: Lys529 is closer to the receptor side of **nova**. This highlights the pivotal role of electrostatic interactions between residues in driving the spectral modulation, further supporting the efficacy of our mutation strategy.

We have designed a new bioluminescent system, **nova-I351D**, which emits light at 1123 nm with an emission intensity approximately 60 % of that of **oLu-WT**, slightly higher than cycLuc1 (50 %) [100]. Given that cycLuc1 has been validated to achieve sufficient brightness for in vivo imaging [100], nova-I351D is anticipated to exhibit comparable or enhanced imaging performance. Furthermore, its emission wavelength in the NIR-II reigon is positioned to avoid the tissue absorption and scattering windows, ensuring optimal sensitivity for luminescent signal detection. In principle, this system is conceptually similar to the way luciferin undergoes a series of reactions within wild-type luciferase to produce BL. In our design, the luciferin analogue, nova luciferin, undergoes a series of reactions within the I351D mutant luciferase to generate BL (Scheme S1).

## 4. Conclusion

This study systematically investigated the effects of electrostatic interactions and extended conjugation on the fluorescence redshift of **oLu**. As a D-A system, oLu shows enhanced redshift upon the introduction of substituents that enhance either its donor or acceptor properties. Furthermore, extending the conjugated π-bridge between the donor and acceptor moieties further promotes the fluorescence redshift. Mutations in the surrounding residues of oLu can also enhance the donor or acceptor properties, contributing to the redshift. Building on these insights, we finally theoretically designed a new red-shifted bioluminescent system, **nova-I351D**, through structural modifications of **oLu** and luciferase mutations. **nova-I351D** emits brigtly in the NIR-II region. It shows the potential for deep tissue imaging, could represents a new-type of bioluminescent probes in NIR-II reigon.

## 5. Author statement

Jinyu Wang did all the calculations and wrote the draft. Deping Hu interpreted the data and improve the manuscript. Ya-Jun Liu has made

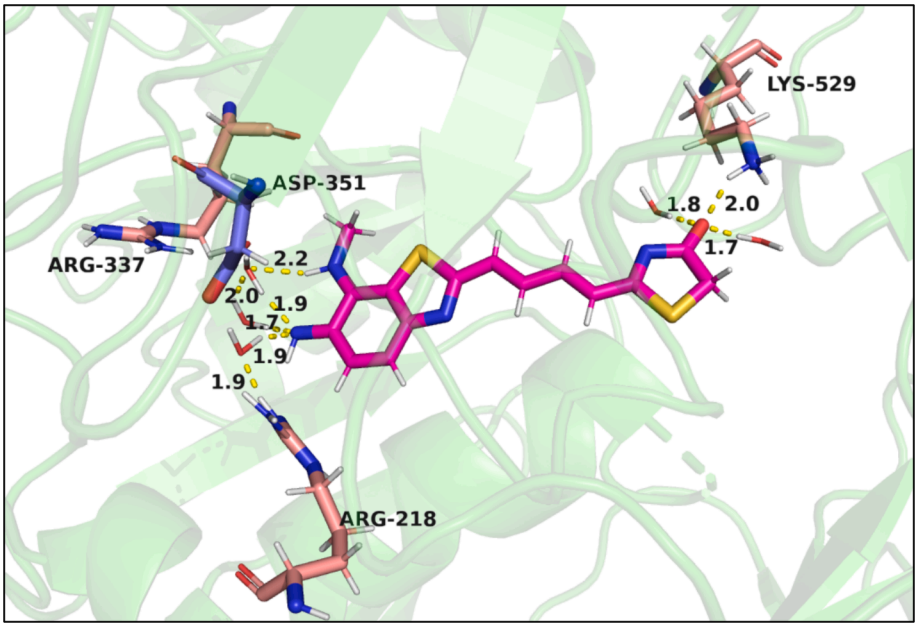


**Fig. 5.** The key substrate-luciferase interactions of nova in the I351D mutant.

contributions to the design of the work and improve the manuscript. We agree to be accountable for all aspects of the work in ensuring the accuracy or integrity of any part of the work.

## CRediT authorship contribution statement

**Jinyu Wang:** Writing – original draft, Investigation, Data curation. **Deping Hu:** Software, Methodology, Formal analysis. **Ya-Jun Liu:** Writing – review & editing, Supervision, Methodology, Formal analysis, Conceptualization.

## Declaration of competing interest

The authors declare that they have no known competing financial interests or personal relationships that could have appeared to influence the work reported in this paper.

## Acknowledgments

The authors acknowledge the support by grants from the National Natural Science Foundation of China (Grant Nos. 22373010 and 22403008) and Beijing Natural Science Foundation (Grant No. 2244074).

## Appendix A. Supplementary data

Supplementary data to this article can be found online at https://doi.org/10.1016/j.jphotochem.2025.116393.

## Data availability

Data will be made available on request.

## References

[1] C. Li, G. Chen, Y. Zhang, et al., Advanced Fluorescence Imaging Technology in the Near-Infrared-II Window for Biomedical Applications, J. Am. Chem. Soc. 142 (2020) 14789–14804, https://doi.org/10.1021/jacs.0c07022.
[2] Y. J. Liu., Understanding the complete bioluminescence cycle from a multiscale computational perspective: A review, J. Photochem. Photobiol. C: Photochem. Rev. 52 (2022), 100537, https://doi.org/10.1016/j.jphotochemrev.2022.100537.
[3] P. Feng, H. Zhang, Q. Deng, W. Liu, et al., Real-Time Bioluminescence Imaging of Nitroreductase in Mouse Model, Anal. Chem. 88 (2016) 5610–5614, https://doi.org/10.1021/acs.analchem.6b01160.
[4] T.N. Demidova, F. Gad, T. Zahra, et al., Monitoring photodynamic therapy of localized infections by bioluminescence imaging of genetically engineered bacteria, J. Photochem. Photobiol. B Biol. 81 (2005) 15–25, https://doi.org/10.1016/j.jphotobiol.2005.05.007.
[5] N. Gaspar, J.R. Walker, G. Zambito, et al., Evaluation of NanoLuc substrates for bioluminescence imaging of transferred cells in mice, J. Photochem. Photobiol. B Biol. 216 (2021) 112128, https://doi.org/10.1016/j.jphotobiol.2005.05.007.
[6] J. Yang, W. Ding, C. Ran, et al., Bioluminescence Imaging with Functional Amyloid Reservoirs in Alzheimer's Disease Models, Anal. Chem. 95 (2023) 14261–14270, https://doi.org/10.1021/acs.analchem.3c02358.
[7] Y.Q. Tang, Y.J. Liu, Theoretical study on bioluminescent mechanism and process of Siberian luminous earthworm Fridericia heliota, J. Photochem. Photobiol. A Chem. 380 (2019) 111870, https://doi.org/10.1016/j.jphotochem.2019.111870.
[8] S.F. Chen, E.S. Vysotski, Y.J. Liu, H(2)O-Bridged Proton-Transfer Channel in Emitter Species Formation in Obelin Bioluminescence, J. Phys. Chem. B 125 (2021) 10452–10458, https://doi.org/10.1021/acs.jpcb.1c03985.
[9] Y. Ando, K. Niwa, N. Yamada, T. Enomoto, T. Irie, H. Kubota, Y. Ohmiya, H. Akiyama, Firefly bioluminescence quantum yield and colour change by pH-sensitive green emission, Nat. Photon. 2 (2007) 44–47, https://doi.org/10.1038/nphoton.2007.251.
[10] Y. Luo, Y.J. Liu, Bioluminophore and Flavin Mononucleotide Fluorescence Quenching of Bacterial Bioluminescence-A Theoretical Study, Chem Eur J 22 (2016) 16243–16249, https://doi.org/10.1002/chem.201603314.
[11] B.W. Ding, P. Naumov, Y.J. Liu, Mechanistic insight into marine bioluminescence: photochemistry of the chemiexcited Cypridina (sea firefly) lumophore, J. Chem. Theory Comput. 11 (2015) 591–599, https://doi.org/10.1021/ct5009203.
[12] J. Vieira, L. Pinto da Silva, J.C. Esteves da Silva, Advances in the knowledge of light emission by firefly luciferin and oxyluciferin, J. Photochem. Photobiol. B Biol. 117 (2012) 33–39, https://doi.org/10.1016/j.jphotobiol.2012.08.017.
[13] W.D. McElroy, H.H. Seliger, E.H. White, Mechanism of bioluminescence, chemiluminescence and enzyme function in the oxidation of firefly luciferin, Photochem. Photobiol. 10 (1969) 153–170, https://doi.org/10.1111/j.1751-1097.1969.tb05676.x.
[14] L. Yue, J.Y. Wang, Y.J. Liu, Free energy simulations unravel luciferin-chirality dependence in firefly bioluminescence-A pKa-controlled asymmetric catalysis, J. Catal. 436 (2024) 115590, https://doi.org/10.1016/j.jcat.2024.115590.
[15] M. Vacher, I. Fdez Galvan, B. W. Ding, S. Schramm, R. Berraud-Pache, P. Naumov, N. Ferre, Y. J. Liu, I. Navizet, D. Roca-Sanjuan, W. J. Baader, R. Lindh, Chemi- and Bioluminescence of Cyclic Peroxides, Chem. Rev. 118 (2018), 6927-6974.
[16] B.R. Branchini, T.L. Southworth, M.H. Murtiashaw, H. Boije, S.E. Fleet, A mutagenesis study of the putative luciferin binding site residues of firefly luciferase, Biochemistry 42 (2003) 10429–10436, https://doi.org/10.1021/bi030099x.
[17] G.R. Reddy, W.C. Thompson, S.C. Miller, Robust light emission from cyclic alkylaminoluciferin substrates for firefly luciferase, J. Am. Chem. Soc. 132 (2010) 13586–13587, https://doi.org/10.1021/ja104525m.
[18] D.K. Sharma, S.T. Adams, K.L. Liebmann, S.C. Miller, Rapid Access to a Broad Range of 6'-Substituted Firefly Luciferin Analogues Reveals Surprising Emitters and Inhibitors, Org. Lett. 19 (2017) 5836–5839, https://doi.org/10.1021/acs.orglett.7b02806.
[19] W. Wu, J. Su, M. Li, et al., cybLuc: An Effective Aminoluciferin Derivative for Deep Bioluminescence Imaging, Anal. Chem. 89 (2017) 4808–4816, https://doi.org/10.1021/acs.analchem.6b03510.
[20] Y. Ikeda, T. Saitoh, K. Suzuki, et al., An allylated firefly luciferin analogue with luciferase specific response in living cells, Chem. Commun. 54 (2018) 1774–1777, https://doi.org/10.1039/c7cc09720d.
[21] K.A. Jones, W.B. Porterfield, C.M. Rathbun, D.C. McCutcheon, M.A. Paley, J. A. Prescher, Orthogonal Luciferase-Luciferin Pairs for Bioluminescence Imaging, J. Am. Chem. Soc. 139 (2017) 2351–2358, https://doi.org/10.1021/jacs.6b11737.
[22] N.R. Conley, A. Dragulescu-Andrasi, J. Rao, W.E. Moerner, A selenium analogue of firefly D-luciferin with red-shifted bioluminescence emission, Angew. Chem. Int. Ed. 51 (2012) 3350–3353, https://doi.org/10.1002/anie.201105653.
[23] R.C. Steinhardt, C.M. Rathbun, J.A. Prescher, et al., Brominated Luciferins Are Versatile Bioluminescent Probes, Chembiochem. 18 (2017) 96–100, https://doi.org/10.1002/cbic.201600564.
[24] B.R. Branchini, Chemical synthesis of firefly luciferin analogs and inhibitors, Methods Enzymol. 305 (2000) 188–195, https://doi.org/10.1016/S0076-6879(00)05488-4.
[25] H. Takakura, K. Sasakura, T. Nagano, et al., Development of luciferin analogues bearing an amino group and their application as BRET donors, Chem. Asian J. 5 (2010) 2053–2061, https://doi.org/10.1002/asia.201000219.
[26] D.C. McCutcheon, M.A. Paley, R.C. Steinhardt, J.A. Prescher, Expedient synthesis of electronically modified luciferins for bioluminescence imaging, J. Am. Chem. Soc. 134 (2012) 7604–7607, https://doi.org/10.1021/ja301493d.
[27] S. Ioka, T. Saitoh, S. Nishiyama, et al., Synthesis of Firefly Luciferin Analogues and Evaluation of the Luminescent Properties, Chemistry 22 (2016) 9330–9337, https://doi.org/10.1002/chem.201600278.
[28] B.S. Zhang, K.A. Jones, D.C. McCutcheon, J.A. Prescher, Pyridone Luciferins and Mutant Luciferases for Bioluminescence Imaging, Chembiochem 19 (2018) 470–477, https://doi.org/10.1002/cbic.201700542.
[29] R.C. Steinhardt, J.M. O'Neill, J.A. Prescher, et al., Design and Synthesis of an Alkynyl Luciferin Analogue for Bioluminescence Imaging, Chem. Eur. J. 22 (2016) 3671–3675, https://doi.org/10.1002/chem.201503944.
[30] S. Iwano, R. Obata, H. Niwa, et al., Development of simple firefly luciferin analogs emitting blue, green, red, and near-infrared biological window light, Tetrahedron 69 (2013) 3847–3856, https://doi.org/10.1016/j.tet.2013.03.050.
[31] Y. Ikeda, T. Nomoto, Y. Hiruta, N. Nishiyama, D. Citterio, Ring-Fused Firefly Luciferins: Expanded Palette of Near-Infrared Emitting Bioluminescent Substrates, Anal. Chem. 92 (2020) 4235–4243, https://doi.org/10.1021/acs.analchem.9b04562.
[32] M. Kiyama, S. Iwano, S.A. Maki, et al., Quantum yield improvement of red-light-emitting firefly luciferin analogues for in vivo bioluminescence imaging, Tetrahedron 74 (2018) 652–660, https://doi.org/10.1016/j.tet.2017.11.051.
[33] M.P. Hall, C.C. Woodroofe, L. Mezzanotte, et al., Click beetle luciferase mutant and near infrared naphthyl-luciferins for improved bioluminescence imaging, Nat. Commun. 9 (2018) 132, https://doi.org/10.1038/s41467-017-02542-9.
[34] A.P. Jathoul, H. Grounds, J.C. Anderson, M.A. Pule, A dual-color far-red to near-infrared firefly luciferin analogue designed for multiparametric bioluminescence imaging, Angew. Chem. Int. Ed. 53 (2014) 13059–13063, https://doi.org/10.1002/anie.201405955.
[35] D.M. Mofford, G.R. Reddy, S.C. Miller, Aminoluciferins extend firefly luciferase bioluminescence into the near-infrared and can be preferred substrates over D-luciferin, J. Am. Chem. Soc. 136 (2014) 13277–13282, https://doi.org/10.1021/ja505795s.
[36] D.R. Caldwell, K.M. Townsend, B. Kolbaba-Kartchner, T. Hadjian, J. Ivanic, A. C. Love, B. Malvar, J. Mills, J.A. Prescher, M.J. Schnermann, Expedient Synthesis and Characterization of pi-Extended Luciferins, J. Org. Chem. 89 (2024) 14625–14633, https://doi.org/10.1021/acs.joc.3c01920.
[37] E.H. White, E. Rapaport, T.A. Hopkins, H.H. Seliger, Chemi- and bioluminescence of firefly luciferin, J. Am. Chem. Soc. 91 (1969) 2178–2180, https://doi.org/10.1021/ja01036a093.

[38] R. Shinde, J. Perkins, C.H. Contag, Luciferin derivatives for enhanced in vitro and in vivo bioluminescence assays, Biochemistry 45 (2006) 11103–111112, https://doi.org/10.1021/bi060475o.
[39] Y.Q. Sun, J. Liu, P. Wang, J. Zhang, W. Guo, D-Luciferin Analogues: a Multicolor Toolbox for Bioluminescence Imaging, Angew. Chem. Int. Ed. 51 (2012) 8428–8430, https://doi.org/10.1002/anie.201203565.
[40] E.H. White, H. Worther, H.H. Seliger, W.D. Mcelroy, Amino Analogs of Firefly Luciferin and Biological Activity Thereof, J. Am. Chem. Soc. 88 (1966) 2015–2019, https://doi.org/10.1021/ja00961a030.
[41] C.H. Chang, D.M. Fontaine, S. Gomez, B.R. Branchini, J.C. Anderson, Synthesis and Bioluminescence of 'V'-Shaped Firefly Luciferin Analogues Based on A Novel Benzobisthiazole Core, Chem. Eur. J. 29 (2023) e202302204, https://doi.org/10.1002/chem.202302204.
[42] R. Ono, K. Osawa, Y. Takahashi, Y. Noguchi, N. Kitada, R. Saito-Moriya, T. Hirano, S.A. Maki, K. Shibata, H. Akiyama, K.-I. Kanno, H. Itabashi, M. Hiyama, Quantum yield of near-infrared bioluminescence with firefly luciferin analog: AkaLumine, J. Photochem. Photobiol. A Chem. 434 (2023) 114270, https://doi.org/10.1016/j.jphotochem.2022.114270.
[43] K.R. Harwood, D.M. Mofford, G.R. Reddy, S.C. Miller, Identification of mutant firefly luciferases that efficiently utilize aminoluciferins, Chem. Biol. 18 (2011) 1649–1657, https://doi.org/10.1016/j.chembiol.2011.09.019.
[44] B. Said Alipour, S. Hosseinkhani, S.K. Ardestani, A. Moradi, The effective role of positive charge saturation in bioluminescence color and thermostability of firefly luciferase, Photochem. Photobiol. Sci. 8 (2009) 847–855, https://doi.org/10.1039/b901938c.
[45] C.M. Colee, N.M. Oberlag, M. Simon, O.S. Chapman, L.C. Flanagan, E.S. Reid-McLaughlin, J.A. Gewing-Mullins, S. Maiche, D.F. Patel, A.R.O. Cavalcanti, A. M. Leconte, Discovery of Red-Shifting Mutations in Firefly Luciferase Using High-Throughput Biochemistry, Biochemistry 63 (2024) 733–742, https://doi.org/10.1021/acs.biochem.3c00708.
[46] V.R. Viviani, G.F. Pelentir, G. Oliveira, A. Tomazini, V.R. Bevilaqua, Role of E270 in pH- and metal-sensitivities of firefly luciferases, Photochem. Photobiol. Sci. 19 (2020) 1548–1558, https://doi.org/10.1039/d0pp00190b.
[47] M.I. Koksharov, N.N. Ugarova, Strategy of mutual compensation of green and red mutants of firefly luciferase identifies a mutation of the highly conservative residue E457 with a strong red shift of bioluminescence, Photochem. Photobiol. Sci. 12 (2013) 2016–2027, https://doi.org/10.1039/c3 pp50242b.
[48] H. Salehi-Sedeh, F. Ataei, S. Jarchi, R. Hamidi, S. Hosseinkhani, Effect of mutation at positively charged residues (K329 and R330) in a flexible region of firefly luciferase on structure and kinetic properties, Enzyme Microb. Technol. 131 (2019) 109424, https://doi.org/10.1016/j.enzmictec.2019.109424.
[49] H. Takakura, Molecular Design of d-Luciferin-Based Bioluminescence and 1,2-Dioxetane-Based Chemiluminescence Substrates for Altered Output Wavelength and Detecting Various Molecules, Molecules 26 (2021) 1618, https://doi.org/10.3390/molecules26061618.
[50] C. Carrasco-Lopez, N.M. Lui, S. Schramm, P. Naumov, The elusive relationship between structure and colour emission in beetle luciferases, Nat. Rev. Chem. 5 (2021) 4–20, https://doi.org/10.1038/s41570-020-00238-1.
[51] S. Liu, Y. Su, M.Z. Lin, J.A. Ronald, Brightening up Biology: Advances in Luciferase Systems for in Vivo Imaging, ACS, Chem. Biol. 16 (2021) 2707–2718, https://doi.org/10.1021/acschembio.1c00549.
[52] W. Zhou, M.P. Valley, J. Shultz, E.M. Hawkins, L. Bernad, T. Good, D. Good, T. L. Riss, D.H. Klaubert, K.V. Wood, New bioluminogenic substrates for monoamine oxidase assays, J. Am. Chem. Soc. 128 (2006) 3122–3123, https://doi.org/10.1021/ja058519o.
[53] W.B. Porterfield, K.A. Jones, D.C. McCutcheon, J.A. Prescher, A "Caged" Luciferin for Imaging Cell-Cell Contacts, J. Am. Chem. Soc. 137 (2015) 8656–8659, https://doi.org/10.1021/jacs.5b02774.
[54] D.M. Mofford, S.T. Adams Jr., G.S. Reddy, G.R. Reddy, S.C. Miller, Luciferin Amides Enable in Vivo Bioluminescence Detection of Endogenous Fatty Acid Amide Hydrolase Activity, J. Am. Chem. Soc. 137 (2015) 8684–8687, https://doi.org/10.1021/jacs.5b04357.
[55] M.X. Navarro, C.K. Brennan, A.C. Love, J.A. Prescher, Caged luciferins enable rapid multicomponent bioluminescence imaging, Photochem. Photobiol. 100 (2024) 67–74, https://doi.org/10.1111/php.13814.
[56] I. Navizet, D. Roca-Sanjuán, L. Yue, Y.J. Liu, N. Ferré, R. Lindh, Are the Bio- and Chemiluminescence States of the Firefly Oxyluciferin the Same as the Fluorescence State? Photochem. Photobiol. 89 (2012) 319–325, https://doi.org/10.1111/php.12007.
[57] B.F. Milne, Red-shifting the optical response of firefly oxyluciferin with group 15/16 substitutions, PCCP 16 (2014) 24971–24977, https://doi.org/10.1039/C4CP04347B.
[58] X.Q. Ran, X. Zhou, J.D. Goddard, The Spectral–Structural Relationship of a Series of Oxyluciferin Derivatives, ChemPhysChem 16 (2014) 396–402, https://doi.org/10.1002/cphc.201402611.
[59] V. Satalkar, E. Benassi, Y. Mao, X. Pan, C. Ran, X. Chen, Y. Shao, Computational investigation of substituent effects on the fluorescence wavelengths of oxyluciferin analogs, J. Photochem. Photobiol. A Chem. 431 (2022) 114018, https://doi.org/10.1016/j.jphotochem.2022.114018.
[60] Y.Y. Cheng, Y.J. Liu, Theoretical Development of Near-Infrared Bioluminescent Systems, Chem. Eur. J. 24 (2018) 9340–9352, https://doi.org/10.1002/chem.201800416.
[61] Y.Y. Cheng, J. Zhu, Y.J. Liu, Theoretical tuning of the firefly bioluminescence spectra by the modification of oxyluciferin, Chem. Phys. Lett. 591 (2014) 156–160, https://doi.org/10.1016/j.cplett.2013.11.023.
[62] R. Berraud-Pache, I. Navizet, QM/MM calculations on a newly synthesised oxyluciferin substrate: new insights into the conformational effect, PCCP 18 (2016) 27460–27467, https://doi.org/10.1039/C6CP02585D.
[63] D.I. Kato, T. Kubo, M. Maenaka, K. Niwa, Y. Ohmiya, M. Takeo, S. Negoro, Confirmation of color determination factors for Ser286 derivatives of firefly luciferase from Luciola cruciata (LUC-G), J. Mol. Catal. B Enzym. 87 (2013) 18–23, https://doi.org/10.1016/j.molcatb.2012.10.009.
[64] M.B. Al-Handawi, S. Polavaram, A. Kurlevskaya, P. Commins, S. Schramm, C. Carrasco-Lopez, N.M. Lui, K.M. Solntsev, S.P. Laptenok, I. Navizet, P. Naumov, Spectrochemistry of Firefly Bioluminescence, Chem. Rev. 122 (2022) 13207–13234, https://doi.org/10.1021/acs.chemrev.1c01047.
[65] P. Naumov, Y. Ozawa, K. Ohkubo, S. Fukuzumi, Structure and spectroscopy of oxyluciferin, the light emitter of the firefly bioluminescence, J. Am. Chem. Soc. 131 (2009) 11590–11605, https://doi.org/10.1021/ja904309q.
[66] L. Yue, Z. Lan, Y.J. Liu, The Theoretical Estimation of the Bioluminescent Efficiency of the Firefly via a Nonadiabatic Molecular Dynamics Simulation, J. Phys. Chem. Lett. 6 (2015) 540–548, https://doi.org/10.1021/jz502305g.
[67] Y.Y. Cheng, Y.J. Liu, What Exactly Is the Light Emitter of a Firefly? J. Chem. Theory Comput. 11 (2015) 5360–5370, https://doi.org/10.1021/acs.jctc.5b00659.
[68] E. Runge, E.K.U. Gross, Density-Functional Theory for Time-Dependent Systems, Phys. Rev. Lett. 52 (1984) 997–1000, https://doi.org/10.1103/PhysRevLett.52.997.
[69] T. Yanai, D.P. Tew, N.C. Handy, A new hybrid exchange–correlation functional using the Coulomb-attenuating method (CAM-B3LYP), Chem. Phys. Lett. 393 (2004) 51–57, https://doi.org/10.1016/j.cplett.2004.06.011.
[70] S. Grimme, J. Antony, S. Ehrlich, H. Krieg, A consistent and accurateab initioparametrization of density functional dispersion correction (DFT-D) for the 94 elements H-Pu, J. Chem. Phys. 132 (2010) 154104, https://doi.org/10.1063/1.3382344.
[71] J.W. Pitera, M. Falta, W.F. van Gunsteren, Dielectric properties of proteins from simulation: The effects of solvent, ligands, pH, and temperature, Biophys. J. 80 (2001) 2546–2555, https://doi.org/10.1016/S0006-3495(01)76226-1.
[72] M.K. Gilson, B.H. Honig, The Dielectric-Constant of a Folded Protein, Biopolymers. 25 (1986) 2097–2119, https://doi.org/10.1002/bip.360251106.
[73] J. Tomasi, B. Mennucci, R. Cammi, Quantum mechanical continuum solvation models, Chem. Rev. 105 (2005) 2999–3093, https://doi.org/10.1021/cr9904009.
[74] M. J. Frisch, G. W. Trucks, H. B. Schlegel, G. E. Scuseria, M. A. Robb, J. R. Cheeseman, G. Scalmani, V. Barone, B. Mennucci, G. A. Petersson, Revision D. 01; Gaussian, Inc.:, C. Wallingford, CT, 2009.
[75] T. Lu, F.W. Chen, Multiwfn: A multifunctional wavefunctionanalyzer, J. Comput. Chem. 33 (2012) 580–592, https://doi.org/10.1002/jcc.22885.
[76] J.A. Sundlov, D.M. Fontaine, T.L. Southworth, et al., Crystal Structure of Firefly Luciferase in a Second Catalytic Conformation Supports a Domain Alternation Mechanism, Biochemistry 51 (2012) 6493–6495, https://doi.org/10.1021/bi300934s.
[77] A. Fiser, A. Sali, ModLoop: automated modeling of loops in protein structures, Bioinformatics 19 (2003) 2500–2501, https://doi.org/10.1093/bioinformatics/btg362.
[78] A. Fiser, R.K.G. Do, A. Sali, Modeling of loops in protein structures, Protein Sci. 9 (2000) 1753–1773, https://doi.org/10.1110/ps.9.9.1753.
[79] R. Anandakrishnan, B. Aguilar, A.V. Onufriev, H++ 3.0: automating pK prediction and the preparation of biomolecular structures for atomistic molecular modeling and simulations, Nucleic Acids Res. 40 (2012) W537–W541, https://doi.org/10.1093/nar/gks375.
[80] V. Hornak, R. Abel, A. Okur, B. Strockbine, A. Roitberg, C. Simmerling, Comparison of multiple Amber force fields and development of improved protein backbone parameters, Proteins 65 (2006) 712–725, https://doi.org/10.1002/prot.21123.
[81] J.M. Wang, R.M. Wolf, J.W. Caldwell, P.A. Kollman, D.A. Case, D.A. Case, Development and testing of a general amber force field, J. Comput. Chem. 25 (2004) 1157–1174, https://doi.org/10.1002/jcc.20035.
[82] P. Cieplak, W.D. Cornell, C. Bayly, P.A. Kollman, Application of the Multimolecule and Multiconformational Resp Methodology To Biopolymers - Charge Derivation for DNA, Rna, and Proteins, J. Comput. Chem. 16 (1995) 1357–1377, https://doi.org/10.1002/jcc.540161106.
[83] I. Navizet, Y.J. Liu, N. Ferré, H.Y. Xiao, W.H. Fang, R. Lindh, Color-Tuning Mechanism of Firefly Investigated by Multi-Configurational Perturbation Method, J. Am. Chem. Soc. 132 (2010) 706–712, https://doi.org/10.1021/ja908051h.
[84] W.L. Jorgensen, J. Chandrasekhar, J.D. Madura, R.W. Impey, M.L. Klein, Comparison of simple potential functions for simulating liquid water, J. Chem. Phys. 79 (1983) 926–935, https://doi.org/10.1063/1.445869.
[85] J.A. Izaguirre, D.P. Catarello, J.M. Wozniak, R.D. Skeel, Langevin stabilization of molecular dynamics, J. Chem. Phys. 114 (2001) 2090–2098, https://doi.org/10.1063/1.1332996.
[86] H.J.C. Berendsen, J.P.M. Postma, W.F. van Gunsteren, A. DiNola, J.R. Haak, Molecular dynamics with coupling to an external bath, J. Chem. Phys. 81 (1984) 3684–3690, https://doi.org/10.1063/1.448118.
[87] T. Darden, D. York, L. Pedersen, Particle mesh Ewald: An N·log(N) method for Ewald sums in large systems, J. Chem. Phys. 98 (1993) 10089–10092, https://doi.org/10.1063/1.464397.
[88] J. Kästner, J.M. Carr, T.W. Keal, W. Thiel, A. Wander, P. Sherwood, DL-FIND: An Open-Source Geometry Optimizer for Atomistic Simulations, Chem. A Eur. J. 113 (2009) 11856–11865, https://doi.org/10.1021/jp9028968.

[89] D.A. Case, H.M. Aktulga, K. Belfon, I.Y. Ben-Shalom, S.R. Brozell, D.S. Cerutti, T. E. Cheatham III, G.A. Cisneros, V.W.D. Cruzeiro, T.A. Darden, R.E. Duke, G. Giambasu, M.K. Gilson, H. Gohlke, A.W. Goetz, R. Harris, S. Izadi, S. A. Izmailov, C. Jin, K. Kasavajhala, M.C. Kaymak, E. King, A. Kovalenko, T. Kurtzman, T.S. Lee, S. LeGrand, P. Li, C. Lin, J. Liu, T. Luchko, R. Luo, M. Machado, V. Man, M. Manathunga, K.M. Merz, Y. Miao, O. Mikhailovskii, G. Monard, H. Nguyen, K.A. O'Hearn, A. Onufriev, F. Pan, S. Pantano, R. Qi, A. Rahnamoun, D.R. Roe, A. Roitberg, C. Sagui, S. Schott-Verdugo, J. Shen, C. L. Simmerling, N.R. Skrynnikov, J. Smith, J. Swails, R.C. Walker, J. Wang, H. Wei, R.M. Wolf, X. Wu, Y. Xue, D.M. York, S. Zhao, P.A. Kollman, Amber 2021, University of California, San Francisco, 2021.

[90] P. Sherwood, A.H. de Vries, M.F. Guest, G. Schreckenbach, C.R.A. Catlow, S. A. French, A.A. Sokol, S.T. Bromley, W. Thiel, A.J. Turner, S. Billeter, F. Terstegen, S. Thiel, J. Kendrick, S.C. Rogers, J. Casci, M. Watson, F. King, E. Karlsen, M. Sjøvoll, A. Fahmi, A. Schäfer, C. Lennartz, QUASI: A general purpose implementation of the QM/MM approach and its application to problems in catalysis, J. Mol. Struct. (Theochem) 632 (2003) 1–28, https://doi.org/10.1016/S0166-1280(03)00285-9.

[91] S. Metz, J. Kästner, A.A. Sokol, T.W. Keal, P. Sherwood, ChemShell-a modular software package for QM/MM simulations, WIREs Comput. Mol. Sci. 4 (2013) 101–110, https://doi.org/10.1002/wcms.1163.

[92] F. Neese, Software update: The ORCA program system-Version 5.0. WIREs Comput. Mol. Sci. 12 (2022), e1606, https://doi.org/10.1002/wcms.1606.

[93] D. Bakowies, W. Thiel, DL_POLY_2.0: A general-purpose parallel molecular dynamics simulation package, J. Mol. Graph. 14 (1996) 136–141, https://doi.org/10.1016/S0263-7855(96)00043-4.

[94] D. Bakowies, W. Thiel, Hybrid models for combined quantum mechanical and molecular mechanical approaches, J. Phys. Chem. 100 (1996) 10580–10594, https://doi.org/10.1021/jp9536514.

[95] Z.Y. Liu, T. Lu, Q.X. Chen, An sp-hybridized all-carboatomic ring, cyclo [18] carbon: Electronic structure, electronic spectrum, and optical nonlinearity, Carbon 165 (2020) 461–467, https://doi.org/10.1016/j.carbon.2020.05.023.

[96] C. Hansch, A. Leo, R.W. Taft, A Survey of Hammett Substituent Constants and Resonance and Field Parameters, Chem. Rev. 91 (1991) 165–195, https://doi.org/10.1021/cr00002a004.

[97] H. Takakura, R. Kojima, Y. Urano, T. Terai, K. Hanaoka, T. Nagano, Aminoluciferins as functional bioluminogenic substrates of firefly luciferase, Chem. Asian J. 6 (2011) 1800–1810, https://doi.org/10.1002/asia.201000873.

[98] K. Zhou, H. Bai, L. Feng, J. Dai, M. Cui, Smart D-π-A Type Near-Infrared Aβ Probes: Effects of a Marked π Bridge on Optical and Biological Properties, Anal. Chem. 89 (2017) 9432–9437, https://doi.org/10.1021/acs.analchem.7b02246.

[99] N. Saleh, A.R. Suwaid, A. Alhalabi, A.Z. Abuibaid, O.V. Maltsev, L. Hintermann, P. Naumov, Bioinspired Molecular Lantern: Tuning the Firefly Oxyluciferin Emission with Host-Guest Chemistry, J. Phys. Chem. B 120 (2016) 7671–7680, https://doi.org/10.1021/acs.jpcb.6b06557.

[100] G. Zambito, N. Gaspar, Y. Ridwan, M.P. Hall, C. Shi, T.A. Kirkland, L.P. Encell, C. Lowik, L. Mezzanotte, Evaluating Brightness and Spectral Properties of Click Beetle and Firefly Luciferases Using Luciferin Analogues: Identification of Preferred Pairings of Luciferase and Substrate for In Vivo Bioluminescence Imaging, Molecular Imaging Biol. 22 (2020) 1523–1531, https://doi.org/10.1007/s11307-020-01523-7.